Available online at www.eccomasproceedia.org
Eccomas Proceedia UNCECOMP (2025) 500-510

ECCOMAS
Proceedia

UNCECOMP 2025
6th ECCOMAS Thematic Conference on
Uncertainty Quantification in Computational Science and Engineering
M. Papadrakakis, V. Papadopoulos, G. Stefanou (eds.)
Rhodes Island, Greece, 15-18 June 2025

COUPLED CANN-DEM SIMULATION FOR HYPERELASTIC SOLIDS

Stefan Hildebrand[1], **Jonathan Georg Friedrich**[1], **and Sandra Klinge**[1]

[1] Department of Structural Mechanics and Analysis, Technische Universität Berlin
Straße des 17. Juni 135, 10623 Berlin, Germany
e-mail: {stefan.hildebrand, sandra.klinge}@tu-berlin.de

Abstract. *A general, unified neural network approach as replacement for the finite element method without the need for analytic expressions for material laws is suggested. The complete simulation process from the material characterization to simulations on a structural level takes place in the new neural network framework. The drawback of many conventional analytic expressions of material laws to require large numbers of experiments for parametrization is addressed by an integrated inverse approach. Specifically, an adaptation of the Deep Energy Method (DEM) is combined with a Constitutive Artificial Neural Network (CANN) and trained on measured displacement fields and prescribed boundary conditions in a coupled procedure. Tests on compressible and incompressible Neo-Hookean solids with up to twelve CANN parameters show high accuracy of the approach and very good generalization of CANNs. A small extent of data is required for robust and reliable training.*

Keywords: Neural Networks, NN, solid mechanics, Constitutive Artificia Neural Networks, CANN, Deep Energy Method, DEM, material modeling, hyperelasticity

ISSN:2623-3339 © 2025 The Authors. Published by Eccomas Proceedia.
Peer-review under responsibility of the organizing committee of UNCECOMP 2025.
doi: 10.7712/120225.12373.21346

1 INTRODUCTION

In computational engineering, machine learning (ML) approaches are gaining increasing attention as alternatives and extensions to traditional simulation techniques [1, 2, 3]. Data-driven methods are successfully used in material modeling [4, 5, 6] and characterization [7, 8], whereas a growing variety of physics-informed methods emerges for the solution of the static equilibrium condition [9, 10, 11]. The present contribution describes the general, unifie neural network approach CANN-DEM [12] for elastostatic simulations. Analytic expressions for the material model [13, 14, 15] are replaced by an Artificia Neural Network (ANN) and an integrated procedure for training based on a small extent of data is suggested to automatize the material characterization. This results in a material-specifi neural solver ready to be used in simulations at the structural level.

The current contribution is structured as follows: Section 2 (Methods and Materials) explains the Neo-Hookean models used in the case studies, as well as the basics of neural methods (CANN and DEM). The proposed setup is outlined in Section 3 (Integration of DEM and CANN). The validation of the proposed setup is shown in Section 4 (Case Study), which is followed by a discussion of advancements, limitations and challenges of implementation in Section 5 (Results). Finally, Section 6 summarizes conclusions and possible future directions of the research work.

2 METHODS AND MATERIALS

2.1 Constitutive modeling of hyperelastic materials

In the hyperelastic theory [16, 17, 18], the material behavior is prescribed by the strain energy density Ψ [19, 20] from which the stress tensor is determined by derivation with respect to the kinematic quantities. In the present contribution, a compressible Neo-Hookean solid is investigated, namely

$$\Psi(I_1, J) \quad = \tfrac{1}{2}\lambda(\log(J))^2 - \mu\log(J) + \tfrac{\mu}{2}(I_1 - 2), \quad \text{for } \mathbf{C} \in \mathbb{R}^{2\times 2} \quad , \tag{1}$$

with I_1 the firs invariant of the right Cauchy-Green tensor $\mathbf{C} = \mathbf{F}^T\mathbf{F}$, $\mathbf{F}$ the deformation gradient and $J = \det \mathbf{F}$. λ and μ are Lamé material parameters that are determined experimentally.

2.2 Artificial Neural Networks (ANNs)

Artificia Neural Networks (ANNs) [21, 22] with parameter set Θ consisting of the weights w and biases b represent arbitrary mappings $\mathcal{R} : \mathbb{R}^n \mapsto \mathbb{R}^m$ [23] with n and m the input and output layer width, respectively. For the DEM, a Fully Connected Neural Network (FCNN) is applied, whereas the CANN requires a custom architecture. The training uses gradient descent based optimization algorithms like Adam. Data-driven loss contributions are computed by means of the Mean Square Error (MSE) function

$$\text{MSE} = \frac{1}{N}\frac{1}{m}\sum_{k=1}^{N}\sum_{i=1}^{m}(R_i(P^k) - \tilde{R}_i(P^k))^2 \quad . \tag{2}$$

Here, P denotes the input to the ANN, R the target output and $\tilde{R}$ the actual ANN output of dimension m with N entries. In the following, quantities denoted with a tilde indicate ANN outputs or quantities that are calculated based on ANN outputs.

2.2.1 The Deep Energy Method (DEM)

The original PINN formulation [24] suggests a loss function based on the squared residual $\mathcal{N}$ of the PDE that is specifie on the collocation points inside the body while the BCs are formulated as another, scaled contribution to the loss function, computed at the collocation points on the boundary [25, 9]. For the solution of coupled problems, several additional terms can be accounted for in the loss function [26]. This approach is adopted by the DEM, which has been introduced specificall for coupled boundary value problems including damage phase fiel modeling and piezoelectricity [27, 28]. Opposite to the standard PINN, the DEM only requires firs derivatives of the displacement fiel $\tilde{\boldsymbol{u}}(\boldsymbol{X})$ to compute the total potential energy Π as the loss function, thus reducing the numerical complexity. The input of the ANN are points in the reference configuratio $\boldsymbol{X} \in B \cup \Gamma$, in the domain B and on its boundary $\Gamma = \Gamma_D \cup \Gamma_N$ consisting of the Dirichlet boundary part Γ_D and the Neumann boundary part Γ_N.

A transformation combines the prescribed displacements on the boundary $\boldsymbol{u}_D(\boldsymbol{X}_D)$, $\boldsymbol{X}_D \in \Gamma_D$ and the ANN output $\tilde{\boldsymbol{z}}(\boldsymbol{X})$ to calculate the displacement fiel $\tilde{\boldsymbol{u}}(\boldsymbol{X})$. To this end, a continuously differentiable mapping $\boldsymbol{A}(\boldsymbol{X})$ independent from the ANN parameters with $\boldsymbol{A}(\boldsymbol{X}_D) = \boldsymbol{0}$ is introduced. In a further step, the definitio of $\boldsymbol{u}_D$ is extended by setting entries corresponding to free collocation points to zero: $\boldsymbol{u}_D(\boldsymbol{X}_F) = 0$, $\boldsymbol{X}_F \in B \cup \Gamma_N$, $\boldsymbol{X}_F \notin \Gamma_D$, such that the displacement fiel reads:

$$\tilde{\boldsymbol{u}}(\boldsymbol{X}) = \boldsymbol{u}_D(\boldsymbol{X}) + \boldsymbol{A}(\boldsymbol{X})\tilde{\boldsymbol{z}}(\boldsymbol{X}) \quad . \tag{3}$$

Accordingly, $\tilde{\boldsymbol{u}}$ fulfill the Dirichlet BCs and is differentiable w.r.t. $\boldsymbol{X}$ so that the NN parameters are are trained as the solution of an unconstrained optimization problem.

The corresponding loss function to minimize is

$$\mathcal{L}^{\mathrm{DEM}}(\tilde{\boldsymbol{u}}) = \tilde{\Pi} = \int_B \left(\Psi\left(\tilde{\boldsymbol{F}}\right) - \boldsymbol{b}\cdot\tilde{\boldsymbol{u}}\right) \mathrm{d}V - \int_{\Gamma_N} \overline{\boldsymbol{T}}\cdot\tilde{\boldsymbol{u}}\,\mathrm{d}A \tag{4}$$

with the deformation gradient $\tilde{\boldsymbol{F}} = \frac{\partial(\boldsymbol{X}+\tilde{\boldsymbol{u}})}{\partial \boldsymbol{X}}$, body forces $\boldsymbol{b}$ and the traction $\overline{\boldsymbol{T}} = \boldsymbol{P}\cdot\boldsymbol{N}$ define as the 1^{st} Piola-Kirchhoff stress tensor $\boldsymbol{P}$ projection on the outward normal N of Γ. The described information fl w is illustrated in Fig. 1.

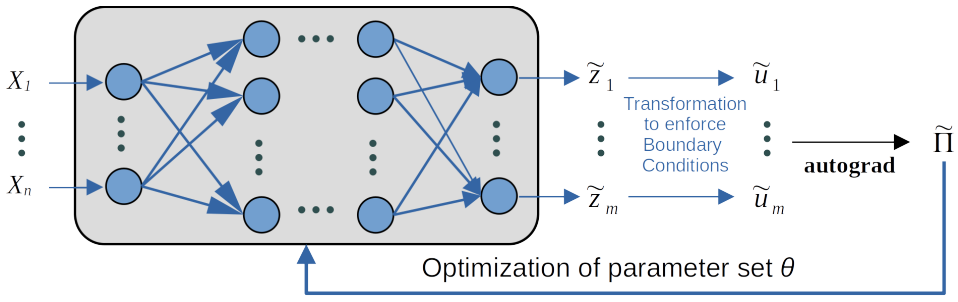

Figure 1: Information fl w in DEM [12].

2.2.2 Constitutive Artificial Neural Networks (CANN)

Constitutive Artificia Neural Networks (CANNs) [29, 30, 31] replace the conventional approach of fittin the stress-strain curves of hyperelastic materials by a manually chosen set of

analytic expressions with a generalized ANN approach. The activation functions in the CANN are oriented on typical function types in conventional hyperelastic material laws and summed up in order to retain polyconvexity. Alternatively, Kolmogorov-Arnold-Networks (KANs) and more generic ANN architectures combined with automatic pruning can be applied [32, 33, 34]

CANN learn the strain energy density Ψ depending on the deformation gradient $\mathbf{F}$ which inherently provides thermodynamic consistency. This way, the firs Piola-Kirchhoff stress tensor can be obtained via autograd according to $\mathbf{P} = \frac{\partial \Psi}{\partial \mathbf{F}}$. On the input side, the invariants of $\mathbf{F}$ are calculated and passed into the ANN which enforces material objectivity, frame indifference, material symmetry and isotropy.

3 A NEW GENERIC ANN-APPROACH FOR SIMULATION IN SOLID MECHANICS: INTEGRATION OF DEM AND CANN IN A NESTED SETUP

In order to replace the analytical expressions for the material model in the DEM, a generic, neural approach is suggested in the following. The aim is to set up a completely automated process which integrates the material characterization and the simulation step and requires only a small number of experiments and no explicit knowledge of an material model. The structure is moreover designed to allow the application of the obtained material model in further simulations. The completely ANN based nature of this approach finall allows to perform the computation on the same highly parallelized and optimized hardware, such as graphics or specialized ML accelerator cards.

3.1 Training stage

In the training stage, the material characterization is carried out in a nested setup of DEM and CANN depicted in Fig. 2 resulting in two nested training loops. Input to the coupled CANN-DEM training are coordinates in the undeformed configuratio $\mathbf{X}$, one or more sets of BCs and the displacements $\mathbf{u}$ of the measured deformation. The inner training of the DEM is run to predict the deformations based on the given BCs and the randomly initialized state of the CANN. From the difference between the DEM output $\tilde{u}_i$ and the measured deformation state u_i caused by the prescribed BCs, the loss value for the outer training of the CANN is calculated as

$$\mathcal{L}_{CANN} = \frac{1}{N} \sum_{i=1}^{N} (u_i - \tilde{u}_i)^2 \tag{5}$$

with N the number of grid points in the geometry. In this setup, every epoch of the CANN training requires training of the DEM to compute the predicted deformations $\tilde{\mathbf{u}}$. Since the CANN values are updated adaptively, the DEM training load is reduced in later epochs of the CANN training, comparable to the process of transfer learning. Fig. 2 shows the detailed structure of the CANN-DEM training stage. During the initial training phase, the DEM network requires significantl more epochs to converge. Even without the CANN optimizer being active, the CANN loss changes significantl during the firs epochs due to variations in the calculated displacement fields This introduces considerable noise in the CANN loss at the beginning of the training, thus jeopardizing the efficien y of the coupled training. To address this issue and better separate the effects of inner and outer training processes, a starting phase is introduced, where the CANN optimizer remains inactive until the last ten CANN losses are below a threshold ($outer\_loss\_conv\_crit$).

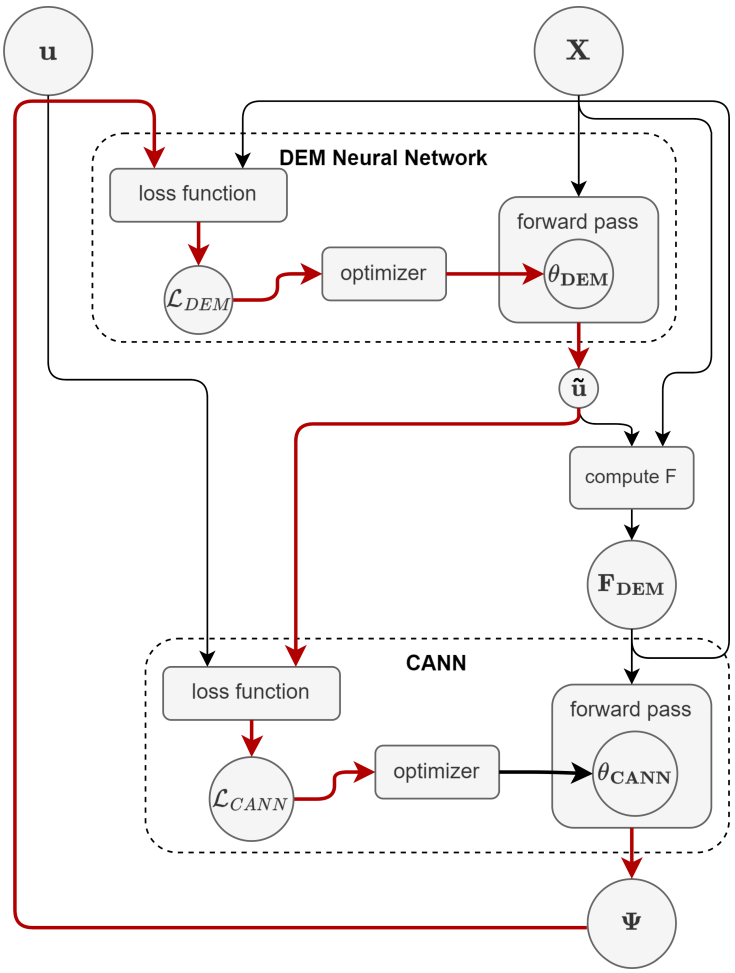

Figure 2: Nested structure of the CANN-DEM. The red path is the calculation path requiring differentiation through the DEM optimization process [12].

3.2 Application stage

After the training, the neural network approach can be used for simulations on the structural level where the inputs are sample points in the new domain as well as both Dirichlet and Neumann BCs. In this stage, the parameters of the CANN stay fi ed and are not anymore subject to optimization. Only the optimizer of the DEM is applied to fin a displacement fiel which satisfie the equilibrium condition based on the corresponding stresses calculated by the CANN. This training is the counterpart of the Newton-Raphson scheme in the FEM and visualized in Fig. 3.

4 CASE STUDY

4.1 Data generation

A multiaxial static tension-testing machine and an optical system to measure the surface displacements of the test specimen as described in [35, 36, 37] is simulated by a conventional run of the DEM in the present study in order to generate the training data. To this end, $N_x = 20, N_y = 5$ equidistant collocation points have been used. The ANN consists of three hidden layers with Tanh activation function with 8 neurons per hidden layer. The accuracy of this setup is investigated on a 2D cantilever beam from [28] that is made of a Neo-Hookean material with

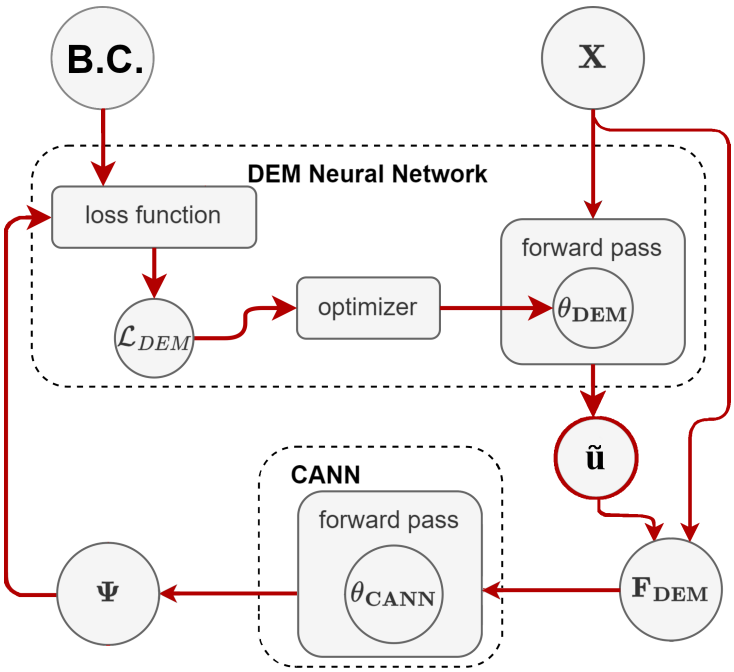

Figure 3: Structure of the CANN-DEM application phase. The CANN parameters are now fi ed [12].

$E = 1000$ Pa and $\nu = 0.3$ and has length $L = 4$ m, height $H = 1$ m and width $D = 1$ m. The beam is clamped at the left side and subjected to a uniform traction load with the resulting force $R = -5.0$ N at the right end.

Note that the training data can also be generated by the traditional FEM, however the DEM simulation allows for direct analysis of the results at the same collocation points, thus facilitating their.

4.2 Hyperparameter

The model requires several hyperparameters to be set in order to run the simulation [12]. Besides conventional values such as the learning rates for the inner and outer optimizer, the layer widths for both ANNs and the numbers of layers and types of activations functions need to be defined The nested setup requires to introduce further parameters such as a convergence criterion for the inner DEM training loop, weighing parameters of the inner against the outer loss function and adapted parameters during the starting phase and to determine when to end the starting phase.

The CANN layer width is varied in the case studies and stated for each numerical sample separately, together with the function that the CANN represents in symbolic form. Similar to [30], the CANN takes the deformation gradient as input, calculates its invariants, then passes them through a mixed layer with linear and quadratic functions, followed by another mixed layer with linear and exponential functions. A fina linear layer combines all values into the scalar value for the strain energy density. The convergence criterion for each DEM training checks if the difference of the last $end\_length = 4$ losses is less than $conv\_crit$.

5 RESULTS

A twelve-parameter CANN with linear, quadratic, and exponential activation functions to capture complex material behaviors is trained based on the compressible Neo-Hookean model,

whereas additional case studies concerned with alternative material types are presented in [12].

The compressible Neo-Hookean model [28] follows the equation

$$\Psi(I_1, J) = \frac{1}{2}\lambda\left(\log(J)\right)^2 - \mu\log(J) + \frac{1}{2}\mu(I_1 - 2) \quad . \tag{6}$$

The prescribed values for the Lamé parameters in the simulated example are $\lambda = 16443\ \frac{\mathrm{N}}{\mathrm{m}^2}$ and $\mu = 336\ \frac{\mathrm{N}}{\mathrm{m}^2}$. The training utilizes six deformation states based on the load cases given in Table 1.

Table 1: The six different load cases used for the twelve parameter CANN-DEM training.

Load case	t_0	t_1	t_2	t_3	t_4	t_5
Load in x-direction / N	0	0	0	100	300	400
Load in y-direction / N	3	-15	50	-50	0	-100

The training process reduced the loss steadily, identifying the material law of the form

$$\begin{aligned}\Psi(I_1, J) = {} & 157.54 \cdot (I_1 - 2) + 0.00 \cdot \left(\exp\left(0.00 \cdot (I_1 - 2)\right) - 1\right) \\ & + 0.00 \cdot (J - 1) + 0.00 \cdot \left(\exp\left(0.00 \cdot (J - 1)\right) - 1\right) \\ & + 2.57 \cdot (I_1 - 2)^2 + 0.00 \cdot \left(\exp\left(0.00 \cdot (I_1 - 2)^2\right) - 1\right) \\ & + 1166.02 \cdot (J - 1)^2 + 600.47 \cdot \left[\exp(5.03 \cdot (J - 1)^2) - 1\right] \quad .\end{aligned} \tag{7}$$

The identifie material model closely approximates the expected factor at the term $(I_1 - 2)$ (Eq. 6) and fina deformations accurately match the numerical surrogate simulations shown in Fig. 4. The stretch-stress behavior confirm that the twelve-parameter CANN (Eq. 7) closely replicates the behavior of the underlying material model over a broad range of deformations.

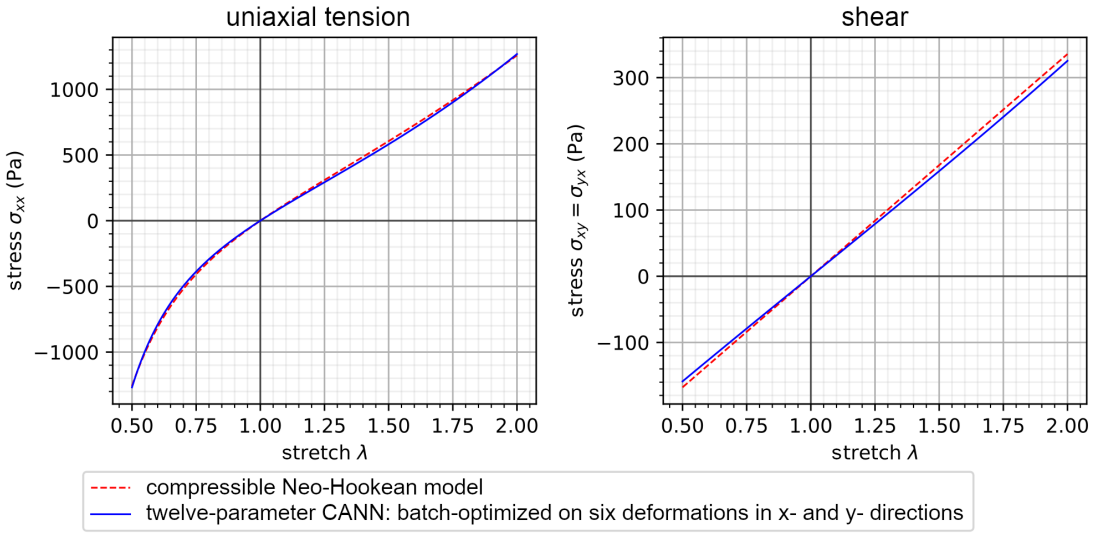

Figure 4: Comparison of stretch-stress behavior between the compressible Neo-Hookean model and the twelve-parameter CANN model trained on six deformations [12].

To assess the generalization capability of the trained twelve-parameter CANN, the approach is tested against three load conditions which are not part of the training data set, namely the

loads at the right end of the beam

$$\mathbf{t}_0 = [0\,\mathrm{N},\ 8\,\mathrm{N}]\,, \quad \mathbf{t}_1 = [100\,\mathrm{N},\ 0\,\mathrm{N}]\,, \quad \mathbf{t}_2 = [200\,\mathrm{N},\ 100\,\mathrm{N}]\,.$$

The results show that the predicted deformations closely match the numerical surrogate simulations (Fig. 5). The calculated loss values are within the same range as during the training.

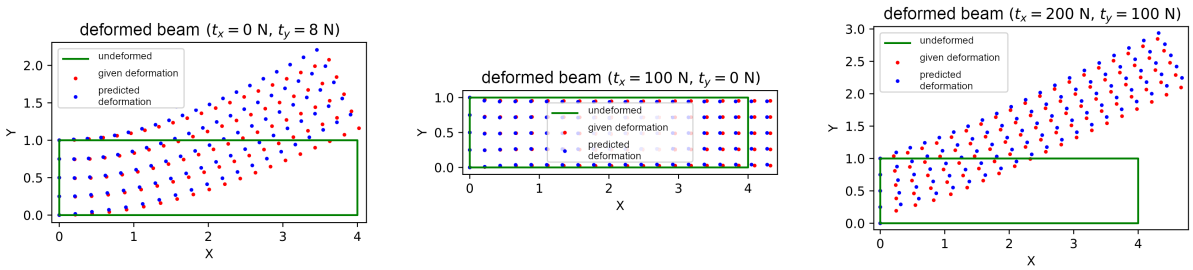

Figure 5: Comparison of the resulting deformation from given material model and predicted material model for three different load conditions that are not used in training [12].

6 CONCLUSIONS

In this study, a generic ANN-approach consisting of DEM and CANN in a nested setup has been investigated for elastostatic simulations. No explicit material model is required, as the CANN replaces analytical expressions to describe the material behavior. The model is trained based on a small number of deformation states and corresponding boundary conditions and can be used in further simulations on a structural level. The test presented in the contribution applies a twelve-parameter CANN for a compressible Neo-Hookean material. The CANN-DEM training has been conducted with six deformation states on 100 sample points.

The achieved results have shown that the coupled CANN-DEM architecture works robustly and performs comparable to a conventional method with an analytical constitutive model. The nested approach is shown to be able to identify hyperelastic material models within a space spanned by up to twelve parameters given training data that incorporates sufficientl different stress-strain states. The test results show a high accuracy in all case studies. Both the given displacement field and the stretch-stress behavior of the given material models are approximated closely. The resulting CANN models generalize well for loading conditions which are not part of the training data. Accordingly, the presented CANN-DEM approach allows to conduct a completely ANN based simulation of structural behavior without a conventional constitutive model. Instead, a data-driven approach based on a small number of experiments is sufficien to reliably depict the material behavior and subsequently perform simulations at the structural level.

In conclusion, the integrated process is promising for application in a fully automatized lab setting, from the specimen to the fina material model and simulation setup. Still, specimen of more complex shape, e.g. containing a hole or an L-shape sample, and more complex loading conditions, which lead to stress concentrations and a variety of multiaxial stress states, are expected to reduce the required number of load cases further [38, 39, 40]. To allow a complete 3D characterization of the material, a multi-camera setup could give the necessary data in a single pass. Moreover, deformation data should be included that contains larger stretches. This could help to reduce unexpected parameter combinations in the resulting CANN model.

REFERENCES

[1] Bock F E, Aydin R C, Cyron C J, Huber N, Kalidindi S R and Klusemann B 2019 *Frontiers in Materials* **6** ISSN 2296-8016 URL https://www.frontiersin.org/articles/10.3389/fmats.2019.00110

[2] Cicirello A 2024 *J. Phys.: Conf. Ser.* **2909** 012034 URL https://doi.org/10.1088/1742-6596/2909/1/012034

[3] Le Clainche et al. 2023 *Aero. Sc. Tech.* 108354 URL https://doi.org/10.1016/j.ast.2023.108354

[4] Shoghi R and Hartmaier A 2024 *Mach. Learn.: Sci. Technol.* **5** 025008 URL https://doi.org/10.1088/2632-2153/ad379e

[5] Hildebrand S and Klinge S 2024 *Mach. Learn.: Sci. Technol.* **5** 045058 URL https://iopscience.iop.org/article/10.1088/2632-2153/ad95da

[6] Rezaei S, Moeineddin A and Harandi A 2024 *Computational Mechanics* **74** 333–366 ISSN 1432-0924 URL https://doi.org/10.1007/s00466-023-02435-3

[7] Shoghi R and Morand L and Helm D and Hartmaier A 2024 *Comp. Mech.* **74** 447-466 URL https://doi.org/10.1007/s00466-023-02440-6

[8] Karabulut M 2025 *Buildings* **15**(3) 432 URL https://doi.org/10.3390/buildings15030432

[9] Chadha C, He J, Abueidda D, Koric S, Guleryuz E and Jasiuk I 2024 *Acta Mechanica* **234** 5975–5998 URL https://doi.org/10.1007/s00707-023-03691-3

[10] Liang Z and Gao H and Li T 2022 *Acta Mechanica* **233** 1739-1755 URL https://doi.org/10.1007/s00707-022-03174-x

[11] Wang Y et al. 2025 *Comp. Meth. Appl. Mech. Eng.* URL https://doi.org/10.1016/j.cma.2024.117518

[12] Hildebrand S and Friedrich J G and Mohammadkhah M and Klinge S 2025 *Mach. Learn.: Sci. Technol.* **6** 015038 URL https://doi.org/10.1088/2632-2153/adaf74

[13] Mohammadkhah M and Klinge S 2023 *Journal of the Mechanical Behavior of Biomedical Materials* **148** 106203 ISSN 1751-6161 URL https://www.sciencedirect.com/science/article/pii/S1751616123005568

[14] Graham M and Klinge S 2024 *Journal of the Mechanical Behavior of Biomedical Materials* **149** 106244 ISSN 1751-6161 URL https://www.sciencedirect.com/science/article/pii/S1751616123005970

[15] Eisenträger J and Naumenko K and Altenbach H 2018 *Acta Mech.* **229** 3051-3068 URL https://doi.org/10.1007/s00707-018-2151-1

[16] Kissas G and Mishra S and Chatzi E and De Lorenzis L 2024 *Comp. Meth. Appl. Mech. Eng.* **428** 177053 URL https://doi.org/10.1016/j.cma.2024.117053

[17] Garai A and Haldar K 2025 *Int. J. Mech. Sc.* **286** 109860 URL https://doi.org/10.1016/j.ijmecsci.2024.109860

[18] Aygün S and Klinge S 2020 *Polymers* **12** ISSN 2073-4360 URL https://www.mdpi.com/2073-4360/12/11/2575

[19] Ali A, Hosseini M and Sahari B B 2010 *American Journal of Engineering and Applied Sciences* **3** 232–239 accessed: 2024-07-05 URL https://thescipub.com/abstract/10.3844/ajeassp.2010.232.239

[20] Kalina K A 2025 *Comp. Meth. Appl. Mech. Eng.* URL https://doi.org/10.1016/j.cma.2024.117725

[21] Abueidda D W, Koric S, Abu Al-Rub R, Parrott C M, James K A and Sobh N A 2021 *European Journal of Mechanics - A/Solids* **372** 113431 URL https://doi.org/10.1016/j.euromechsol.2022.104639

[22] Hildebrand S and Klinge S 2024 *Neural Computing and Applications* **36** 16657-16682 URL https://doi.org/10.1007/s00521-024-10132-2

[23] Hornik K 1991 *Neural Networks* **4** 251–257 URL https://www.sciencedirect.com/science/article/pii/089360809190009T

[24] Raissi M, Perdikaris P and Karniadakis G 2019 *Journal of Computational Physics* **378** 686–707 ISSN 0021-9991 URL https://www.sciencedirect.com/science/article/pii/S0021999118307125

[25] Wang S, Teng Y and Perdikaris P 2021a *SIAM Journal on Scientific Computing* **43** A3055–A3081 (*Preprint* https://doi.org/10.1137/20M1318043) URL https://doi.org/10.1137/20M1318043

[26] Goswami S, Anitescu C and Rabczuk T 2020 *Theoretical and Applied Fracture Mechanics* **107** 102527 ISSN 0167-8442 URL https://www.sciencedirect.com/science/article/pii/S0167844219306858

[27] Samaniego E, Anitescu C, Goswami S, Nguyen-Thanh V, Guo H, Hamdia K, Zhuang X and Rabczuk T 2020 *Comp. Meth. Appl. Mech. Eng.* **362** 112790 ISSN 0045-7825 URL https://www.sciencedirect.com/science/article/pii/S0045782519306826

[28] Nguyen-Thanh V M, Zhuang X and Rabczuk T 2020 *European Journal of Mechanics - A/Solids* **80** 103874 ISSN 0997-7538 URL https://www.sciencedirect.com/science/article/pii/S0997753819305352

[29] Peirlinck M, Linka K, Hurtado J A and Kuhl E 2024 *Comp. Meth. Appl. Mech. Eng.* **418** 116534 ISSN 0045-7825 URL https://www.sciencedirect.com/science/article/pii/S0045782523006588

[30] Linka K and Kuhl E 2023 *Comp. Meth. Appl. Mech. Eng.* URL https://www.sciencedirect.com/science/article/pii/S0045782522006867

[31] Linka K, Hillgärtner M, Abdolazizi K P, Aydin R C, Itskov M and Cyron C J 2021 *Journal of Computational Physics* **429** 110010 URL https://www.sciencedirect.com/science/article/pii/S0021999120307841

[32] Abdolazizi K P and Aydin R C and Cyron C J and Linka K 2025 *arXiv* URL https://doi.org/10.48550/arXiv.2502.05682

[33] Fuhg J N and Jones R E and Bouklas N 2024 *Comp. Meth. Appl. Mech. Eng.* URL https://doi.org/10.1016/j.cma.2024.116973

[34] Schommartz J O and Klein D K and Alzate Cobo J C and Weeger O 2025 *Comp. Meth. Appl. Mech. Eng.* **435**117592 URL https://doi.org/10.1016/j.cma.2024.117592

[35] Cooreman S, Lecompte D, Sol H, Vantomme J and Debruyne D 2008 *Experimental Mechanics* **48**(4) 421–433 ISSN 1741-2765 URL https://doi.org/10.1007/s11340-007-9094-0

[36] Polanco-Loria M, Daiyan H and Grytten F 2012 *Polymer Engineering & Science* **52** 438–448 URL https://4spepublications.onlinelibrary.wiley.com/doi/abs/10.1002/pen.22102

[37] Zhao J, Dong J, Liu Z and Xie H 2019 *Polymer Testing* **79** 106015 ISSN 0142-9418 URL https://www.sciencedirect.com/science/article/pii/S0142941819309213

[38] Flaschel M, Kumar S and De Lorenzis L 2022 *npj Computational Materials* **8** ISSN 2057-3960 URL https://doi.org/10.1038/s41524-022-00752-4

[39] Thakolkaran P *et al.* 2022 *arXiv* (*Preprint* 2205.06664) URL https://arxiv.org/abs/2205.06664

[40] Jeong I, Cho M, Chung H and Kim D N 2024 *Comp. Meth. Appl. Mech. Eng.* **418** 116569 URL https://www.sciencedirect.com/science/article/pii/S004578252300693X